Structure determination of chemisorbed $c(2\times2)$P/Fe(100) using angle-resolved photoemission extended fine structure and self-consistent-field $X\alpha$ scattered-wave calculations: Comparison with $c(2\times2)$S/Fe(100)

W. R. A. Huff

Lawrence Berkeley National Laboratory, Berkeley, California 94720
and Department of Chemistry, The University of California, Berkeley, California 94720

Y. Chen

Department of Chemistry and Physics, Pennsylvania State University, University Park, Pennsylvania 16802

X. S. Zhang

Department of Physics, Zhejiang University, Hangzhou, People's Republic of China

L. J. Terminello

Lawrence Livermore National Laboratory, Livermore, California 94550

F. M. Tao and Y. K. Pan

Department of Chemistry, Boston College, Chestnut Hill, Massachusetts 02167

S. A. Kellar and E. J. Moler

Lawrence Berkeley National Laboratory, Berkeley, California 94720
and Department of Chemistry, The University of California, Berkeley, California 94720

Z. Hussain

Lawrence Berkeley National Laboratory, Berkeley, California 94720

H. Wu

Department of Physics, The University of Hong Kong, Hong Kong

Y. Zheng

Oplink, San Jose, California 95131

X. Zhou

Department of Chemistry and Physics, Pennsylvania State University, University Park, Pennsylvania 16802

A. E. Schach von Wittenau

Lawrence Livermore National Laboratory, Livermore, California 94550

S. Kim

Korea Institute of Technology, Taejon, Choongchungnam-do 300-31, Republic of Korea

Z. Q. Huang

James Franck Institute, University of Chicago, Chicago, Illinois 60637

Z. Z. Yang

Institute of Theoretical Chemistry, Jilin University, Changchun, People's Republic of China

D. A. Shirley

Department of Chemistry and Physics, Pennsylvania State University, University Park, Pennsylvania 16802
(Received 3 September 1996)

0163-1829/97/55(16)/10830(11)/$10.00

Angle-resolved photoemission extended fine structure (ARPEFS) was used to determine the structure of $c(2\times2)$P/Fe(100). Photoemission data were collected normal to the (100) surface and 45° off-normal along the [011] direction at room temperature. A close analysis of the autoregressive linear-prediction-based Fourier transform indicates that the P atoms adsorb in the high-coordination fourfold hollow sites. Curved-wave multiple-scattering calculations confirmed the fourfold hollow adsorption site. The P atoms were determined to bond 1.02 Å above the first layer of Fe atoms and the Fe-P-Fe bond angle is 140.6°. Additionally, it was determined that there was no expansion of the Fe surface. Self-consistent-field $X\alpha$ scattered-wave calculations were performed for the $c(2\times2)$P/Fe(100) and the $c(2\times2)$S/Fe(100) systems. These independent results are in excellent agreement with this P/Fe structure and the S/Fe structure previously published, confirming the ARPEFS determination that the Fe_1-Fe_2 interlayer spacing is contracted from the bulk value for S/Fe but not for P/Fe. Finally, this structure is compared to structures from the literature of atomic nitrogen, atomic oxygen, and sulfur adsorbed on the Fe(100) surface. [S0163-1829(97)06715-5]

I. INTRODUCTION

From the viewpoint of materials science, catalysis, and magnetism, a detailed knowledge of iron and its interaction with other elements and compounds is very important. There have been many theoretical studies of the structure and embrittlement of iron grain boundaries due to the presence of phosphorus, a common impurity.[1–5] The electronic and magnetic properties of Fe surfaces and thin films have been studied extensively as well.[6–11] Egert and Panzner[6] seem to be the first to observe the $c(2\times2)$ low-energy electron diffraction (LEED) pattern when P is adsorbed on the Fe(100) surface, but the structure determination using LEED I-V curves has not been done to date to our knowledge.

The structures of atomic nitrogen,[12] atomic oxygen,[13,14] and sulfur[15–17] adsorbed on the Fe(100) surface have been published. Using angle-resolved photoemission extended fine structure (ARPEFS), we present a structure determination of chemisorbed $c(2\times2)$P/Fe(100). These four adsorbate structures are summarized and compared in the Discussion.

Also known as scanned energy photoelectron diffraction,[18] ARPEFS is a technique proven to yield accurate, local structural information of atomic and molecular adsorbates on single-crystal surfaces to very high precision.[17,19–24] In addition to determining the adsorbate structure, ARPEFS is able to detect any relaxation of the first few layers of the substrate. By analyzing the autoregressive linear-prediction- (ARLP) based Fourier transform (FT),[25,26] the binding site and a reasonably accurate structure can be determined. This allows for a close estimate of the structure without the need for any theoretical calculations. Using this estimate as a starting point, curved-wave multiple scattering calculations can then be used to determine the structure to very high precision ($\sim\pm0.02$ Å).

Photoemission data were collected normal to the (100) surface and 45° off-normal along the [011] direction at room temperature. A close analysis of the ARLP-based FT indicates that the P atoms adsorb in the high-coordination fourfold hollow sites. The curved-wave multiple-scattering calculations that simulate the photoelectron diffraction confirmed the fourfold hollow adsorption site. By simultaneously fitting both ARPEFS data sets, the P atoms were determined to bond 1.02 Å above the first layer of Fe atoms. The Fe-P-Fe bond angle is thus 140.6°. Assuming the radius of the Fe atoms is 1.24 Å, the effective P radius is 1.03 Å. To test this fitting method, each data set was fit individually and these results were in good structural agreement.

Additionally, self-consistent-field $X\alpha$ scattered wave (SCF $X\alpha$ SW or $X\alpha$ SW) calculations were performed for the $c(2\times2)$P/Fe(100) and the $c(2\times2)$S/Fe(100) (Ref. 17) systems. These independent results are in excellent agreement with this P/Fe structure and the S/Fe structure previously published, confirming the ARPEFS determination that the Fe_1-Fe_2 interlayer spacing is contracted from the bulk value for S/Fe but not for P/Fe.

II. EXPERIMENT

The experiments were performed in an ultrahigh-vacuum chamber[27] at pressures $\leqslant$60 nPa using beamline 3-3 [Jumbo, the Ge(111) double-crystal monochromator[28]] at the Stanford Synchrotron Radiation Laboratory. This beamline was chosen so that photoemission data could be acquired from the P 1s core level, which has a binding energy of 2149 eV. The photon energy was scanned from 2200 to 2700 eV, the energy resolution was 1.0–2.0 eV full width at half maximum (FWHM), and the degree of linear polarization was $\sim$0.98.

The Fe crystal (6 mm diameter and 2 mm thick) was cut from a boule using an electronic discharge machine. The (100) surface was oriented to $\pm1°$ precision by Laue backscattering. Before chemical etching, the final polishing was accomplished with a 0.5-μm mesh Al_2O_3 powder. The sample was mounted on a high precision (x,y,z,θ,ϕ) manipulator.

The crystal was cleaned by repetitive cycles of Ar^+ ion sputtering (beam voltage 1.0 kV, emission current 20 mA) and subsequent annealing by electron bombardment from behind to $\sim$970 K. Iron undergoes a bcc to fcc phase transition at $\sim$1180 K so it was important not to approach this temperature. The temperature was monitored with a chromel-alumel thermocouple attached near the sample and calibrated with an infrared pyrometer. After 5 weeks of these sputter-anneal cycles, the near-surface region was depleted of C, O, and S, and the surface could be cleaned after each set of experiments by sputtering with a 0.5-kV beam voltage and annealing to only $\sim$820 K.

The LEED pattern of the clean surface showed a clear and sharp (1×1) pattern. The bulk contaminants C, O, and S were monitored with Auger electron spectroscopy (AES) us-

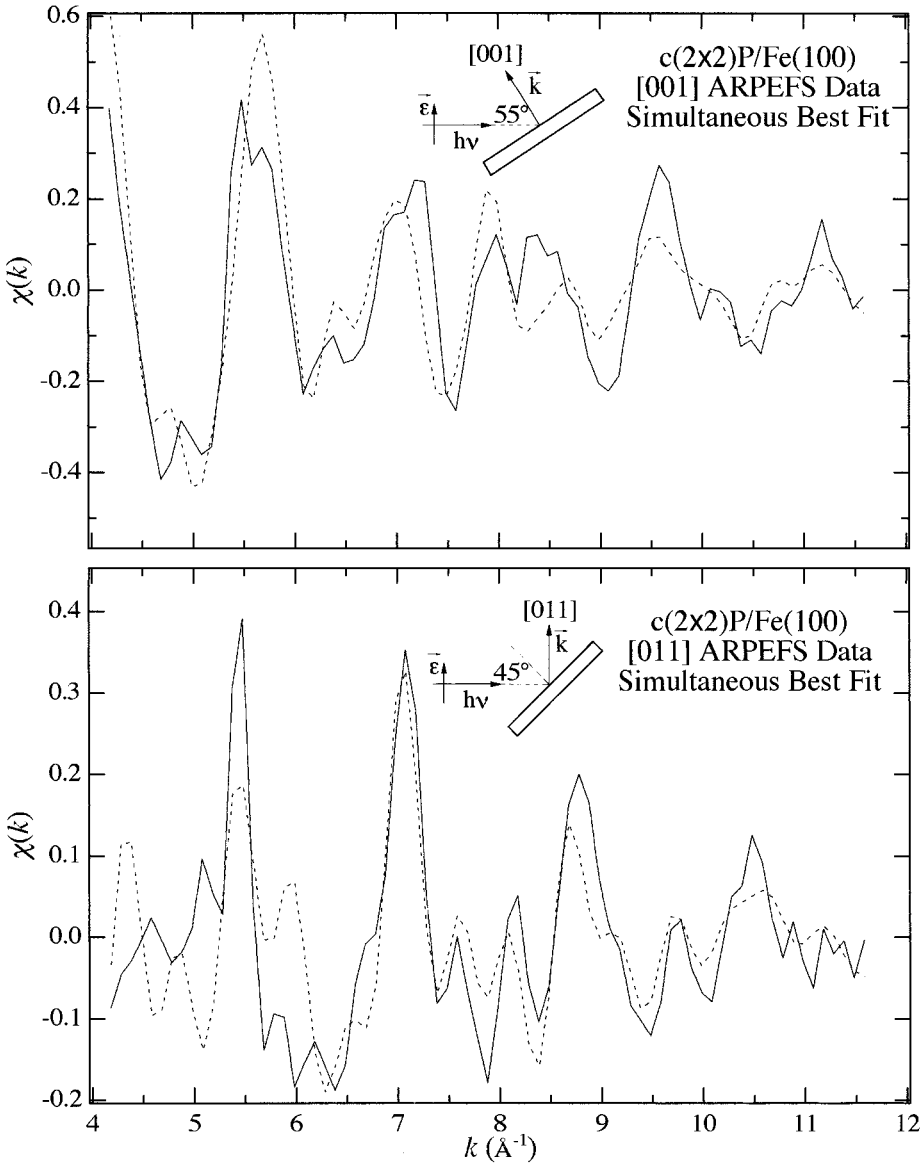

FIG. 1. ARPEFS $\chi(k)$ data for $c(2\times2)$P/Fe(100) in the [001] and [011] directions. Also, schematics of each experimental geometry are shown. The dashed lines are the best-fit multiple-scattering modeling calculation results obtained by fitting both data sets simultaneously.

ing four-grid LEED optics in the retarding field mode. The surface contamination level was within the noise level of the measurements both before and after the data acquisition. The $c(2\times2)$ phosphorus overlayer was prepared by exposing the surface to PH_3 gas (from Matheson Inc.) using an effusive beam doser and then annealing the sample to 770 K. In segregation studies of P in Fe, Shell and Rivière[29] obtained an Auger peak ratio of $P_{LMM}(119\ \text{eV})/Fe_{L_3VV}(47\ \text{eV})=0.932$ whereas Egert and Panzner[6] who observed the $c(2\times2)$ LEED pattern obtained the Auger peak ratio $P_{LMM}/Fe_{L_3VV}=1.0$. For the data presented here, the Auger peak ratio was $P_{LMM}/Fe_{L_3VV}=1.45$.

The photoemission spectra were collected using an angle-resolving electrostatic hemispherical electron energy analyzer (mean radius of 50 mm), which is rotatable 360° around the sample's vertical axis and 100° around the sample's horizontal axis. The analyzer pass energy was set to 160 eV and the energy resolution was approximately 1.6 eV FWHM. The angular resolution of the double einzel input lens was ±3°.

III. DATA ACQUISITION AND ANALYSIS

The photoemission data were collected in two different experimental geometries. In the first data set, the photoemission angle was normal to the Fe(100) surface, i.e., the [001] direction, and the photon polarization vector was 35° from the surface normal. This geometry gives information that is most sensitive to the Fe atoms directly below the P atoms. It could be a first layer Fe atom if P adsorbs in an atop site or a second layer Fe atom if P adsorbs in a fourfold hollow site. If P adsorbs in a bridge site, then the data will be very different. The second set of photoemission data was collected along the [011] direction, i.e., 45° off normal toward the (110) crystallographic plane, and the photon polarization vector was oriented parallel to the emission angle. By taking ARPEFS data off normal, the structure parallel to the surface is enhanced. Thus, curves from the three possible adsorption sites listed above will appear significantly different. Analyzed together, the two different experimental geometries allow for an accurate determination of interlayer spacings, bond lengths, and bond angles.

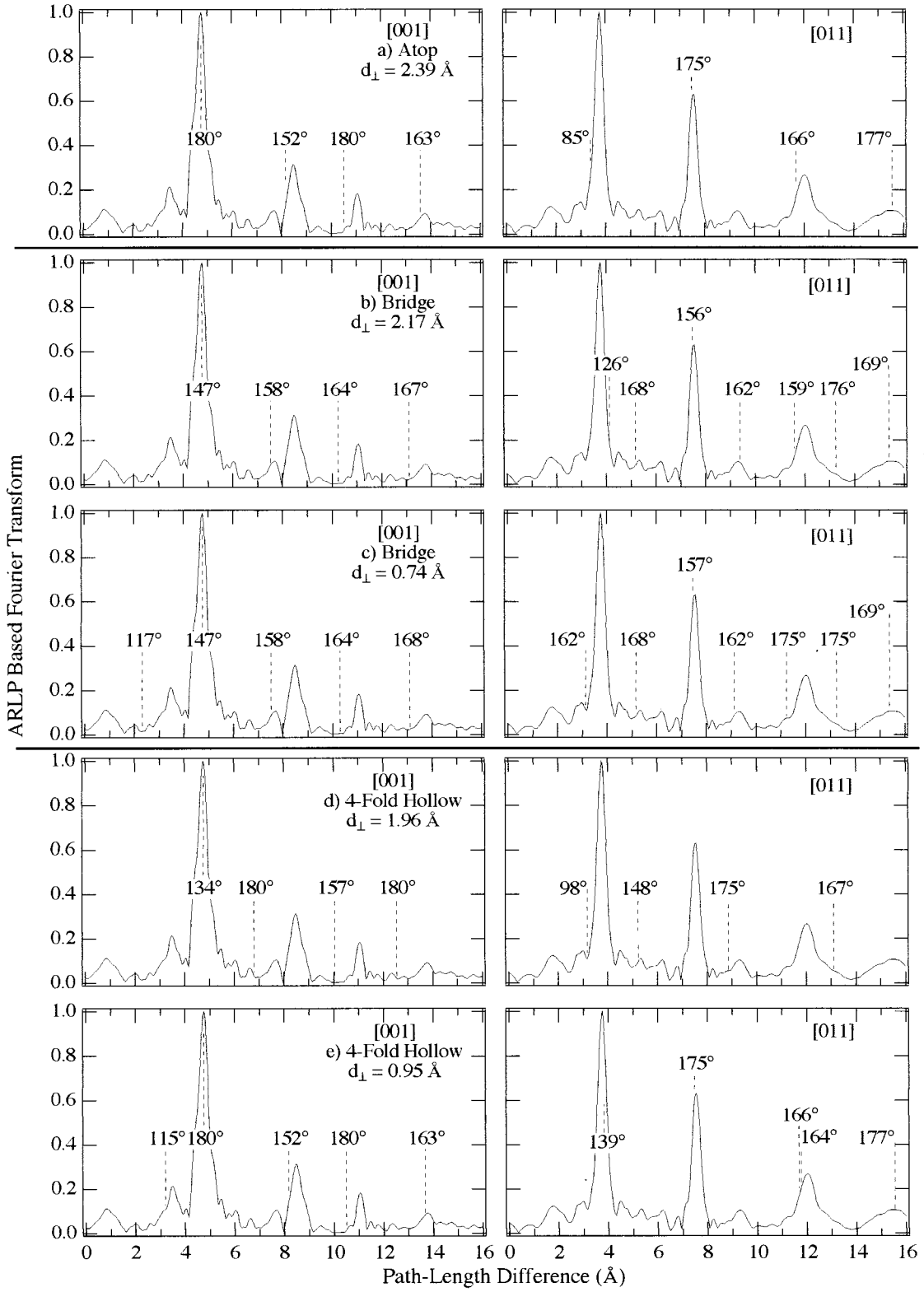

FIG. 2. ARLP-based FT's of the ARPEFS [001] data (left column) and [011] data (right column). The dashed vertical lines indicate the expected peak positions based on calibration to the [001] peak at 4.77 Å for (a) atop, $d_\perp = 2.39$ Å; (b) bridge, $d_\perp = 2.17$ Å; (c) bridge, $d_\perp = 0.74$ Å; (d) fourfold hollow, $d_\perp = 1.96$ Å; (e) fourfold hollow, $d_\perp = 0.95$ Å. The numbers with units of degrees indicate the scattering angles representative of each respective line. Considering both the expected positions and the scattering angles, (e) is most likely the closest estimation to the true structure.

ARPEFS raw data are a series of photoemission spectra with changing photoelectron kinetic energy, which was varied from 60 to 600 eV (4 to 12.5 $Å^{-1}$, recorded in equal 0.1-$Å^{-1}$ steps). Each photoemission spectrum was a 20-eV window with the P 1*s* photopeak located at the center. The peak was fit with a Voigt function to model the natural linewidth as well as the experimental broadening.[30]

The purpose of fitting the spectra is to extract the most

accurate area from the peaks to construct the $\chi(k)$ diffraction curve containing the structural information. $\chi(k)$ is defined by[31]

$$\chi(k)=\frac{I(k)}{I_0(k)}-1, \tag{1}$$

where $I(k)$ is the peak area plotted as a function of the peak position in k space. $I_0(k)$ is a smooth, slowly varying function with an oscillation frequency much lower than $I(k)$ and stems from the contribution of the inelastic scattering processes and the varying atomic cross section. It is adequate to use a simple polynomial function of energy to fit $I_0(k)$.[30] The experimental ARPEFS data thus obtained are plotted in Fig. 1 along with a schematic of the respective experimental geometries. The dashed curves in Fig. 1 are the best-fit results from the multiple scattering modeling calculations, which will be discussed later.

A. Fourier analysis

At this point, it is interesting to take the autoregressive linear-prediction-based Fourier transform (ARLP FT) to move from momentum space to real space. In ARPEFS, the positions of the strong peaks in ARLP FT's from adsorbate-substrate systems can be predicted with fairly good accuracy using the single-scattering cluster (SSC) model together with the concept of strong backscattering from atoms located within a cone around 180° from the emission direction. The effective solid angle of this backscattering cone is ca. 30°–40°; it is not unique, but is operationally defined simply by opening the angle until it can account for the observed FT peaks based on the crystal geometry. Signals from scattering atoms very close to the source atom may be observable even if the scatterers lie outside the nominal backscattering cone.

These FT peaks correspond to path-length differences (PLD), ΔR_j, between the component of the photoemitted wave that propagates directly to the detector and the components that are first scattered by the atomic potentials within this backscattering cone.[19] Thus, the peak positions are

$$\Delta R_j=r_j(1-\cos\theta_j)+\phi_j, \tag{2}$$

where r_j is the bond length, θ_j is the scattering angle (180° for exact backscattering), and ϕ_j is the atomic scattering phase shift. The scattering takes place inside the crystal and the ARPEFS data must be shifted from the measured $\chi(k_{\text{outside crystal}})$ to $\chi(k_{\text{inside crystal}})$ to account for the inner potential. In ARPEFS modeling calculations, the inner potential is treated as an adjustable parameter and is typically 0–15 eV. The inner potential for $c(2\times2)$S/Fe(100) was determined to be 14.5 eV.[17] Thus, before Fourier transformation, the ARPEFS data presented here were shifted by 14 eV to higher kinetic energy.

Without knowing anything about the structure, an analysis of the normal and off-normal ARLP FT's can yield insight into the adsorption site as well as into the bond distance. The sharp $c(2\times2)$ LEED pattern suggests that the monolayer coverage is 50% and that the P atoms adsorb on a high-symmetry site such as atop, bridge, or fourfold hollow. Using the bulk Fe interlayer spacing, 1.43 Å, the strong peak at 4.77 Å in the [001] FT can be used as a calibration to calculate the distance between the P layer and the first Fe layer for each adsorption site. This estimation ignores the small phase shift effects. The PLD for the strong scattering events can then be calculated and the results for each adsorption site can compared to the [001] and [011] data FT's as is done in Fig. 2. The dashed vertical lines in Fig. 2 indicate expected peak positions for each respective geometry. The numbers with units of degrees indicate the scattering angles representative of these lines.

The calculated peak positions for the atop adsorption site are shown in Fig. 2(a). Using the [001] FT peak at 4.77 Å for calibration, the P-Fe_1 interlayer spacing would be 2.39 Å. Calculating prominent PLD's shows reasonable agreement for the [001] FT except there is no way to account for the feature at 3.50 Å. Although the peak positions are in agreement, examining the [011] FT shows that an atop adsorption site is unlikely because the strongest feature in the data is the peak at 3.76 Å. The only Fe atom giving rise to this PLD would be at a scattering angle $\theta_j=85°$. Since ARPEFS is dominated by backscattering events,[19,25] the data peak at 7.57 Å should dominate the FT if P adsorbs in an atop geometry.

When considering a bridge adsorption site, there are two possible P-Fe_1 interlayer spacings, depending on which atom one chooses for calibration of the 4.77-Å [001] data peak. Figure 2(b) indicates a spacing of 2.17 Å obtained if one believes that scattering from the *first* layer Fe atoms gives rise to this peak. Figure 2(c) indicates a spacing of 0.74 Å obtained if one believes that scattering from the *second* layer Fe atoms gives rise to this peak. In each case, only one of two possible bridge sites can be occupied with a $c(2\times2)$ LEED pattern. These sites are degenerate for the [001] FT but become distinct for the [011] FT. For the off-normal case, the strong backscattering peak will be either from a first layer Fe atom or from a second layer Fe atom. Due to the symmetry of the (100) crystal face, each bridge site is energetically degenerate. Thus, in an experimental situation, domains of each will occur and [011] ARPEFS data from $\theta=45°$, $\phi=0°$ would be identical to ARPEFS data where $\theta=45°$, $\phi=90°$. The FT would show peaks from each domain. Therefore, if P adsorbed onto a bridge site, many more peaks would be expected in the [011] FT than are actually there. What this discussion implies is that ARPEFS is unable to distinguish the two domains of $c(2\times2)$ from a $p(1\times1)$ coverage in which both bridge sites were occupied equally. Unless, of course, the adsorbate-adsorbate interaction significantly affects the adsorbate-substrate bonding in the denser coverage.

As with the bridge site, two P-Fe_1 interlayer spacings are possible with the fourfold hollow site. If the data peak at 4.77 Å is due to scattering from a *first* layer Fe atom, then the layer spacing would be 1.96 Å. These calculated PLD are shown in Fig. 2(d). However, if this were the correct geometry, an intense peak due to backscattering from the second layer Fe atoms is expected at 6.79 Å. Additionally, the [011] FT would be dominated by a backscattering PLD at 5.22 Å. The scattering angle for the line at 3.19 Å would be 98°, which is not expected to be so strong as described above.

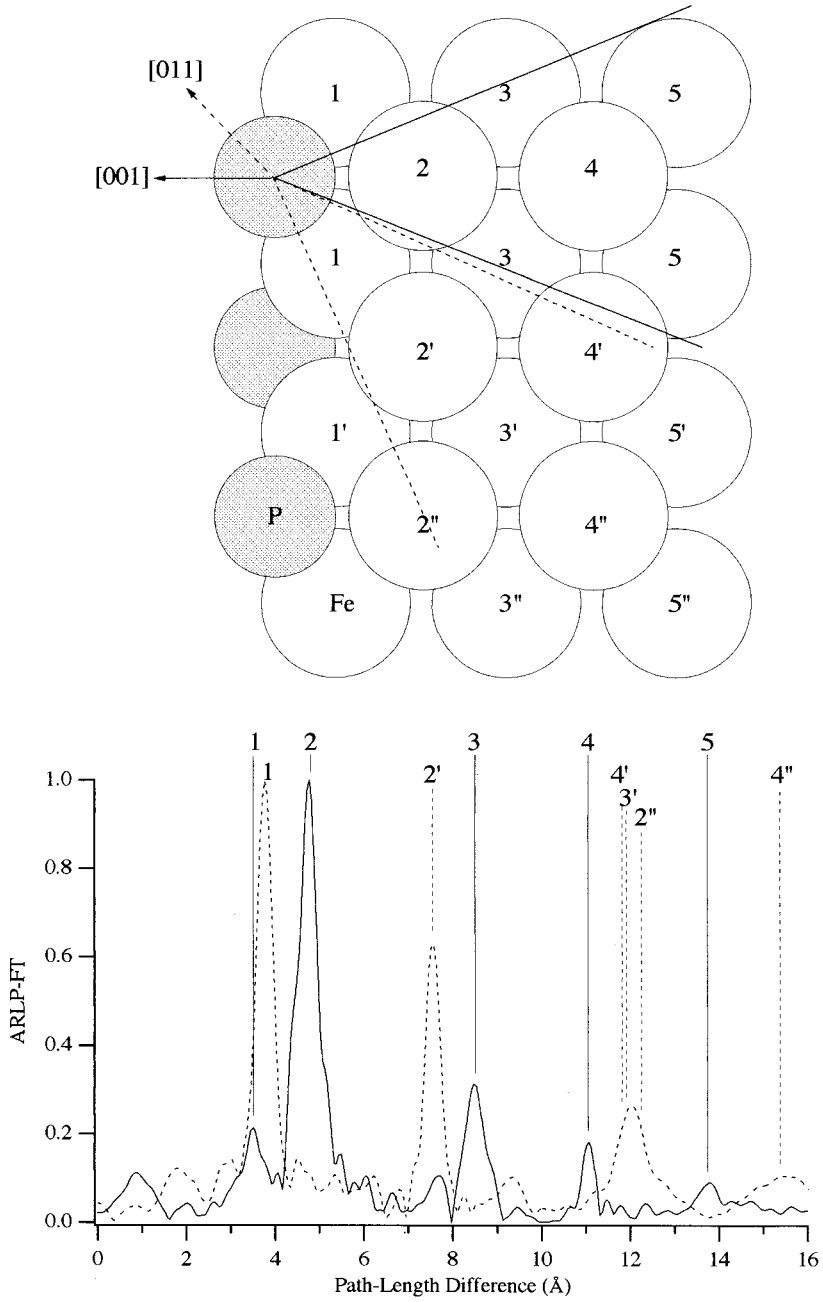

FIG. 3. ARLP-based FT's of the ARPEFS [001] data (solid line) and [011] data (dashed line). A model of the lattice with the backscattering cones for each emission direction indicates the scattering atoms corresponding to the FT peaks.

Alternatively, if the P adsorbs in a fourfold hollow site and the data peak at 4.77 Å is due to backscattering from the *second* layer Fe atoms, then the P-Fe_1 interlayer spacing would be 0.95 Å. These calculated PLD are shown in Fig. 2(e). For this proposed geometry, the calculated PLD are in good agreement with the data and the scattering angles are reasonable for the relative strengths of each peak.

In fact, from the structure analysis of $c(2\times2)$S/Fe,[15–17] it is expected that the P atoms adsorb in the fourfold hollow sites and are ~1 Å above the first layer Fe atoms. It is possible to extend this estimate by calibrating the P-Fe_1 interlayer spacing to each strong data peak and then averaging the results. Doing this estimation, the P-Fe_1 interlayer spacing would be 1.19 Å. Noting that this distance is significantly expanded over the S/Fe value of 1.09 Å (Ref. 17) and that this process neglects phase shifts, one should realize that 1.19 Å is probably too large.

Modeling calculations to be described in the next section are necessary to obtain highly precise bond distances. However, with no modeling calculations, it has already been determined that P adsorbs in the high coordination fourfold hollow sites and the P-Fe_1 interlayer spacing is between 0.95 and 1.19 Å. The ARLP-FT's for both the [001] and the [011] data sets are presented in Fig. 3. Also shown in Fig. 3 is a schematic of the crystal with the backscattering cone for each emission direction superimposed; the labeled atoms correspond to labeled peaks in each FT. The solid lines indicate the scattering atoms for [001] photoemission while the dashed lines indicate the scattering atoms for [011] photoemission. Peaks arise in the FT due to scattering from atoms up to five layers below the emitting atoms. The depth sensitivity of ARPEFS has been described previously[32] and was found to be enhanced by multiple-scattering effects.

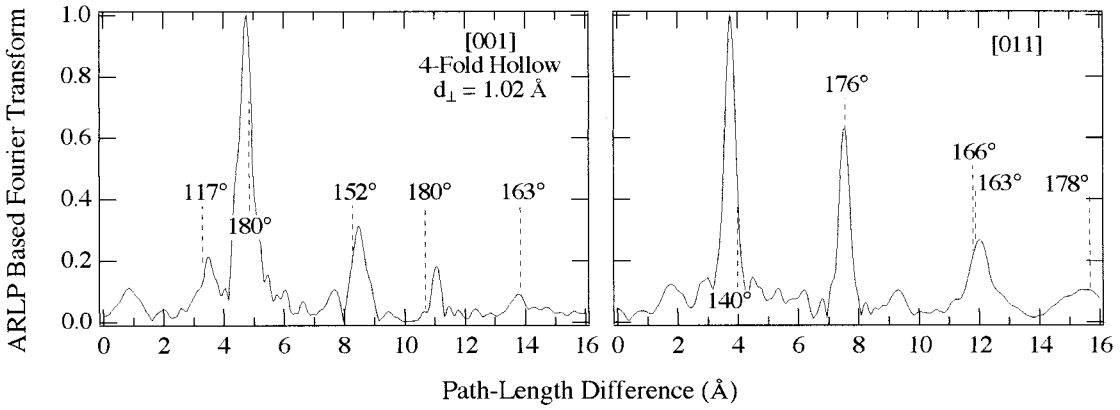

FIG. 4. Directly analogous to Fig. 2(e). Here, $d_{\perp}=1.02$ Å as determined from the multiple-scattering calculations.

B. Multiple-scattering analysis

Modeling calculations were performed to simulate the ARPEFS $\chi(k)$ curve and obtain a structure more precise than yielded by the FT analysis. Using the single-scattering model of ARPEFS,[19,31] $\chi(k)$ can be written as

$$\chi(k)=\sum_j A_j(k)\cos[k(R_j-R_j\cos\theta_j)+\phi_j], \qquad (3)$$

where $A_j(k)$ contains experimental geometry factors including the photon polarization direction and the electron emission direction as well as the scattering amplitude, aperture integration, and thermal averaging.

A code developed by Chen, Wu, and Shirley[33] based on the Rehr-Albers formalism[34] was used for the multiple-scattering spherical-wave calculations presented here. This code differs from the Kaduwela-Fadley code[35] and is sufficiently fast that multicurve fitting calculations can be performed.

The calculations require both structural and nonstructural input parameters. The initial structural parameters were determined from the FT analysis. The nonstructural parameters included were the initial state, the atomic-scattering phase shifts, the crystal temperature, the inelastic mean free path, the emission, and polarization directions, the electron analyzer acceptance angle, and the inner potential. The fitting procedure allowed the structure to vary as well as the inner potential such that a best fit was obtained.

To account for vibration effects of the bulk atoms, the mean square relative displacement (MSRD) was calculated using Eq. (33) by Sagurton, Bullock, and Fadley,[36]

$$\langle u_i^2\rangle \propto \frac{1}{M_i\theta_{D,i}}\left(1+\frac{cT^2}{\theta_{D,i}^2}L\right), \qquad (4)$$

where M_i is the atomic mass, $\theta_{D,i}$ is the correlated Debye temperature, T is the sample temperature, and c is a coefficient that varies slowly with temperature. For calculating the MSRD of the bulk Fe atoms, $\theta_{D,i}$ was set to 400 K.

Accounting for the surface atomic vibration is not as straightforward. The relation between the MSRD and different atomic masses has been given by Allen, Alldredge, and de Wette:[37]

$$\langle u_i^2\rangle\sqrt{M_i}=\langle u_j^2\rangle\sqrt{M_j} \quad (T\approx 0\ \text{K}), \qquad (5)$$

$$\langle u_i^2\rangle=\langle u_j^2\rangle \quad (T\to\infty). \qquad (6)$$

Correlating Eqs. (5) and (6) with Eq. (4), an effective surface atomic mass is introduced such that

$$\langle u_{i,\text{bulk}}^2\rangle\sqrt{M_{i,\text{bulk}}}\cong\langle u_{j,\text{surface}}^2\rangle\sqrt{M_{j,\text{effective}}}, \qquad (7)$$

where $M_{j,\text{effective}}=M_{j,\text{surface}}$ if $T/\theta_{D,i}\ll 1$ or $M_{j,\text{effective}}=M_{j,\text{bulk}}$ if $T/\theta_{D,i}>1$. For $T/\theta_{D,i}\approx 1$, $M_{j,\text{effective}}$ is allowed to vary between the surface and bulk atomic masses. For this study, where $T=300$ K and $\theta_{D,i}=400$ K, it was found that the calculated $\chi(k)$ diffraction curve was insensitive to the surface atomic mass, so $M_{j,\text{effective}}$ was set to the atomic mass of P, 31 a.u.

The atomic-scattering phase shifts were calculated *in situ* by using the atomic potentials tabulated by Moruzzi, Janak, and Williams.[38] The emission and polarization directions and the electron analyzer acceptance angle were set to match the experiment as described earlier. The inelastic mean free path (IMFP) was included using the exponential damping factor $e^{-r/\lambda}$, where λ was calculated using the Tanuma, Powell, and Penn (TPP-2) formula.[39] The IMFP calculation is important in obtaining a close fit to the data and in determining the depth sensitivity of ARPEFS. The TPP-2 formula seems to be the most accurate method to determine the IMFP, especially below 200 eV.

The ''multicurve fitting'' feature means that multiple data curves can be fit simultaneously as explained later. Figure 1 illustrates the best fit (dashed lines) to both the [001] and the [011] ARPEFS data sets (solid lines) by simultaneous fitting. For these fits, a 76-atom cluster was used and the P-Fe_1 interlayer spacing was determined to be 1.02(2) Å. The inner potential was 15.0 eV. The fitting also determined that there was no relaxation of the first or second Fe layers from the bulk 1.43-Å interlayer spacing.

Each data curve was also fitted individually to compare the results. For the [001] individual fit, a 76-atom cluster was used and the P-Fe_1 interlayer spacing was determined to be 1.02(2) Å. For the [011] individual fit, a 75-atom cluster was used and the P-Fe_1 interlayer spacing was determined to be 1.01(2) Å. The inner potential was the same as with the simultaneous fits. Neither of the individual fits showed any relaxation of the first two Fe layers. These results confirm the validity of the multicurve fitting method.

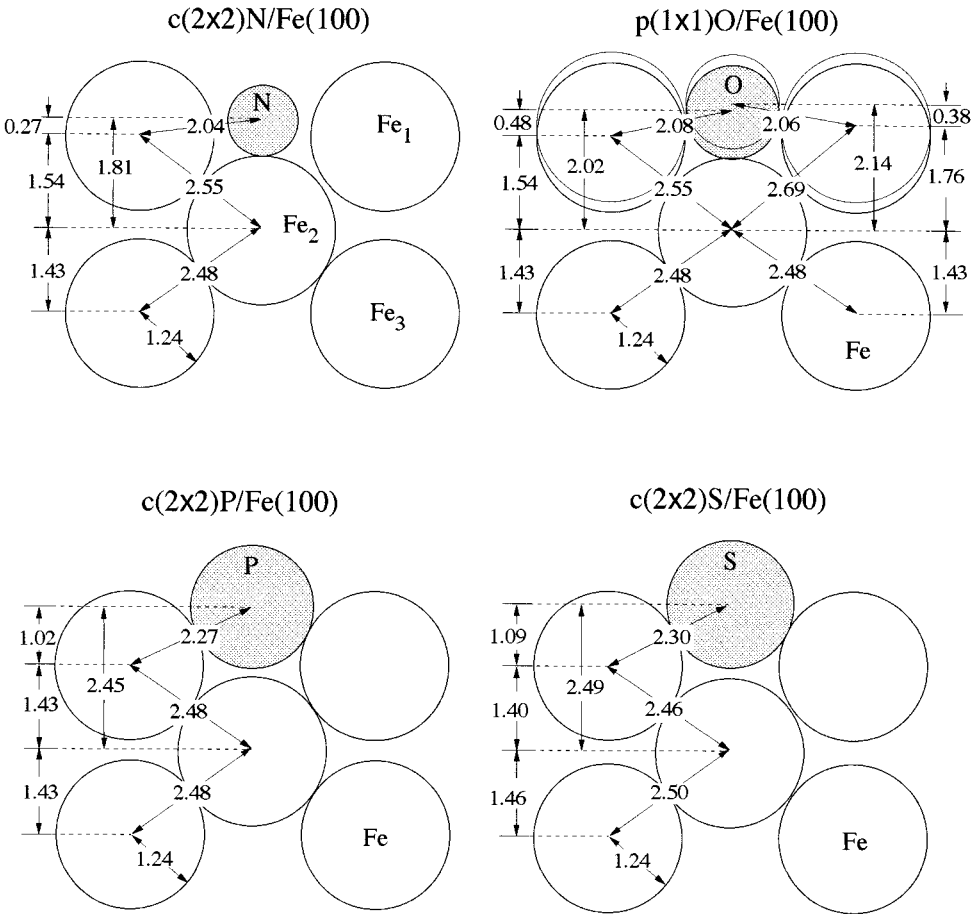

FIG. 5. Schematics of the structures of atomic $c(2\times2)$N/Fe(100), atomic $p(1\times1)$O/Fe(100) (experiment on left, theory on right), $c(2\times2)$P/Fe(100), and $c(2\times2)$S/Fe(100).

For completeness, this modeling result can be compared to the data using the same Fourier analysis presented in Fig. 2. Figure 4 shows the calculated peak positions and their respective scattering angles based on a 1.02-Å P-Fe_1 interlayer spacing; this is directly analogous to Fig. 2(e). Recall that in Fig. 2(e), the 4.77-Å peak in the [001] ARLP-FT was used as a calibration to determine a 0.95-Å P-Fe_1 interlayer spacing. The slight P-Fe_1 expansion from 0.95 to 1.02 Å shifts the calculated FT positions to higher path-length differences. This results in a moderately better overall match to the [001] and [011] experimental data.

The fourfold hollow adsorption site and the P-Fe_1 interlayer spacing for this $c(2\times2)$P/Fe(100) structure correlate well with the structure for chemisorbed $c(2\times2)$S/Fe(100).[15–17] These two structures are compared with atomic $c(2\times2)$N/Fe(100) (Ref. 12) and atomic $p(1\times1)$O/Fe(100) (Refs. 13 and 14) in Fig. 5. These four elements border each other on the periodic table and their interaction with iron is very important in materials science, catalysis, and magnetism.

In Table I, a summary of these four structures is presented along with the structure of the clean Fe(100) surface.[17,40] The structure of atomic O adsorbed on the Fe(100) surface is interesting because the coverage is $p(1\times1)$, unlike atomic N, P, or S. Also, using first-principles calculations, Chubb and Pickett[14] predict a very large expansion of the first layer Fe atoms. A smaller (by a factor of 3) but significant expansion was experimentally determined by Legg *et al.* using LEED.[13] Figure 5 shows a schematic of both proposed oxygen structures (experiment on left, theory on right) as well as the structures for N, P, and S. Because of its ability to accurately determine the near-surface reconstruction of the substrate, ARPEFS should be used to study the $p(1\times1)$O/Fe(100) structure.

C. Discussion of error

The best fit is determined by an R-factor minimization. A three-step fitting process is used to determine the true R-factor minimum to prevent convergence to a local minimum. The initial coarse-fitting minimizes the $\tilde{R}$ factor, $\tilde{R}=R_a$, where

$$R_a=\frac{\Sigma_i[\chi_{i,c}(k)-\chi_{i,e}(k)]^2}{\Sigma_i[\chi^2_{i,c}(k)+\chi^2_{i,e}(k)]}, \tag{8}$$

using a simple net search.[33] $\chi_{i,c}(k)$ and $\chi_{i,e}(k)$ are the points in the calculated and experimental $\chi(k)$ curves, respectively. Second, the code again minimizes $\tilde{R}=R_a$ using the downhill simplex method in multidimensions.[41] Finally, the code minimizes $\tilde{R}=R$ where

$$R=\frac{\Sigma_i[\chi_{i,c}(k)-\chi_{i,e}(k)]^2}{\Sigma_i\chi^2_{i,e}(k)}, \tag{9}$$

TABLE I. Structures of clean Fe(100), $c(2\times2)$N/Fe(100), $p(1\times1)$O/Fe(100), $c(2\times2)$P/Fe(100), and $c(2\times2)$S/Fe(100). For the Fe_1-Fe_2 interlayer spacing, the percent expansion from the 1.43-Å bulk value is indicated. For O/Fe, the upper value indicates the experimental results (Ref. 13) while the lower value indicates the theoretically predicted structure (Ref. 14). ''*X*'' indicates the adsorbate.

	Clean surface	Atomic nitrogen	Atomic oxygen[b]	Phosphorus	Sulfur
Coverage		$c(2\times2)$	$p(1\times1)$	$c(2\times2)$	$c(2\times2)$
$r_{\text{eff}}[X]$ (Å)		0.59	0.78	1.03	1.06
r_{eff}[Fe] (Å)	1.24	1.24	1.24	1.24	1.24
$d_\perp[X-\text{Fe}_1]$ (Å)		0.27	0.48 0.38	1.02	1.09
$d_\perp[\text{Fe}_1-\text{Fe}_2]$ (Å)	1.41 (−1.4%)[a]	1.54 (+7.7%)	1.54 (+7.7%) 1.76 (+23%)	1.43	1.40 (−2.1%)
$d_\perp[\text{Fe}_2\text{-Fe}_3]$ (Å)	1.43	1.43	1.43	1.43	1.46 (+2.1%)
$d_\perp[X-\text{Fe}_2]$ (Å)		1.81	2.02 2.14	2.45	2.49
Bond angle Fe-*X*-Fe		164.8°	153.3° 158.7°	140.6°	123.4°

[a]Percent expansion from the bulk 1.43-Å value.

[b]Upper value from Ref. 13, lower value from Ref. 14.

using the nonlinear Marquardt method.[41]

When using the multicurve fitting feature, $\tilde{R}$ factors from each fit must be considered. For this, the sum of the individual $\tilde{R}$ factors, $\tilde{R}_{\text{total}}$, is used. Thus, if fitting N ARPEFS curves simultaneously, then

$$\tilde{R}_{\text{total}}=\sum_j \frac{1}{N}\tilde{R}_j . \tag{10}$$

Note that the code is flexible such that a weighted sum could be used if justification could be made for giving preference to the $\tilde{R}$ factor of one ARPEFS curve over another.

While fitting, the largest effects stem from changes in the inner potential and the P-Fe_1 interlayer spacing. Figure 6 shows a contour plot of the R factor as the inner potential and P-Fe interlayer spacing are varied. Analysis of Fig. 6 indicates that the precision of ARPEFS is $\sim\pm0.02$ Å, but only if the inner potential is known very well. If, however, the inner potential is allowed to float without constraint, the precision of ARPEFS drops to $\sim\pm0.03$ Å.

IV. SCF $X\alpha$ SW CALCULATIONS

The chemisorption structure of $c(2\times2)$P/Fe(100) and $c(2\times2)$S/Fe(100) (Ref. 17) from the experimental determination may be further confirmed by theoretical calculations in an appropriate model. In this section, we present SCF $X\alpha$ SW (or $X\alpha$ SW) calculations on two atomic clusters, PFe_9 and SFe_9, which represent the two chemisorption systems P/Fe and S/Fe, respectively.

The SCF $X\alpha$ SW formalism developed by Slater[42] and Johnson[43,44] seems to be a convenient compromise between the need for rigorous calculations and the limitations of computing resources. The SCF equation is solved numerically. Basis sets are utilized only in the sense that there is a choice of maximum l value allowed on each center. The numerical solution is made possible by the $X\alpha$ approximation for the exchange contribution to the total potential and the muffin-tin approximation for molecular potential and charge densities. Studies of a range of molecular properties have shown that this method has better performance than semiempirical MO methods and gives results of roughly double-ζ *ab initio* quality.[45–50] The tremendous orbital sizes in our clusters make *ab initio* methods virtually impossible to apply and so the $X\alpha$ SW method is the highest level of theory practically available for this work. In fact, the $X\alpha$ SW method is particularly appropriate because of the high symmetry of the clusters for the calculations.

Due to the limitations of the muffin-tin approximation, the $X\alpha$ SW method may not provide a very accurate calculation of reaction energetics such as the adsorption energy of the P/Fe or S/Fe system. However, the error introduced by the

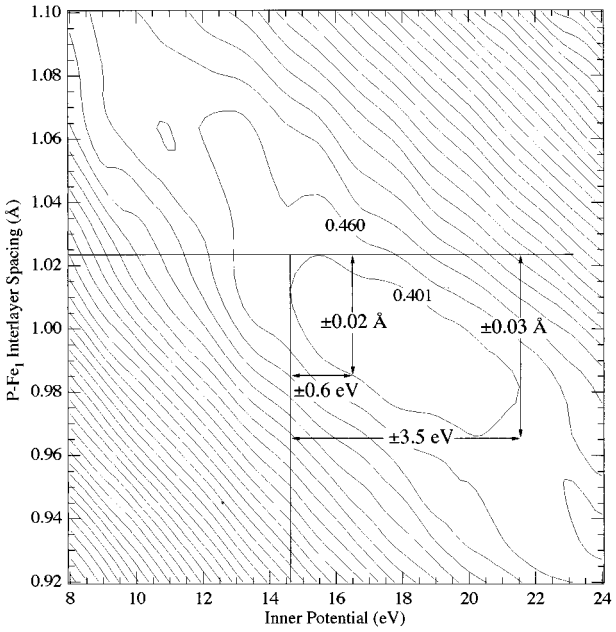

FIG. 6. Contour plot showing how the R factor varies with the P-Fe_1 interlayer spacing and the inner potential when simultaneously fitting the [001] and [011] ARPEFS data.

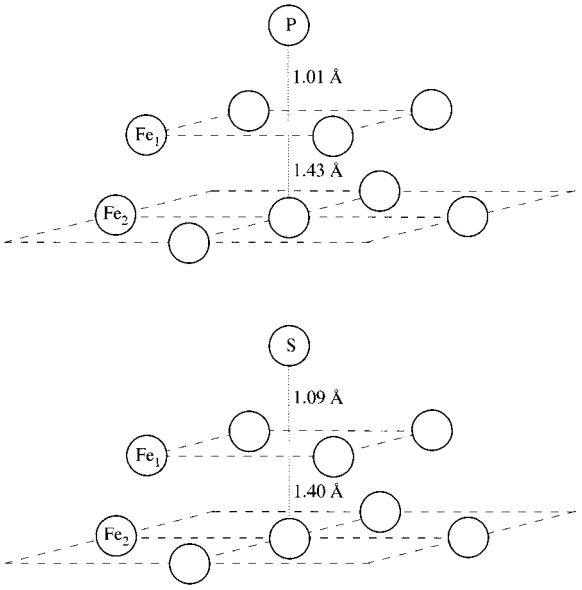

FIG. 7. Structure of the two clusters PFe_9 and SFe_9 used for the $X\alpha$ SW calculations.

muffin-tin approximation can be overcome to some extent by the use of overlapping atomic spheres.[51] We therefore expect that the relative changes of the total energy can be described to desirable accuracy, especially those involved in small structural variations near the equilibrium positions. Of course, the standard parameters should be used for this purpose and the predicted equilibrium structures should not be sensitive to the values of the parameters.

All standard nonempirical parameters for the calculations were used. The radii of atomic spheres were chosen according to Norman[52] and the α exchange parameters were taken from Schwarz's[53] tabulations. In the intersphere and outersphere regions, an average value of α, obtained from a valence-weighted average of the α's for the atoms in the cluster, is employed. Figure 7 shows the structures of the two clusters PFe_9 and SFe_9. The overall symmetry for each cluster is C_{4v}. The four Fe atoms in the top layer are labeled by Fe_1 and the five Fe atoms in the second layer are labeled by Fe_2. The distance of the adsorbed atom P (or S) to the plane formed by the Fe_1 atoms is P-Fe_1 (or S-Fe_1) and the distance between the first and the second layers of Fe atoms is Fe_1-Fe_2. The total energies of the clusters were calculated at several P-Fe_1 (S-Fe_1) distances embracing the experimental equilibrium distance while the Fe_1-Fe_2 interlayer distance was kept at the experimental value. The total energy for a different Fe_1-Fe_2 interlayer distance was also calculated at the experimental P-Fe_1 (S-Fe_1) distance to compare the structural difference in the Fe_1-Fe_2 layer between the P/Fe and the S/Fe systems. The calculation results are presented in Tables I and II for PFe_9 and SFe_9, respectively.

It is seen in Table II that the P-Fe_1 interlayer distance at the energy minimum is around 1.01 Å with the Fe_1-Fe_2 interlayer distance set at the bulk value of 1.43 Å. This result is consistent with the experimentally obtained structure. Table III similarly shows good agreement between the calculations and experiment for the S/Fe (Ref. 17) system where the S-Fe_1 interlayer distance at the energy minimum is around 1.09 Å with the Fe_1-Fe_2 interlayer distance set at the experimentally determined value of 1.40 Å.

TABLE II. Variations of the total energy and the relative energy of PFe_9 with the P-Fe_1 interlayer distance from $X\alpha$ SW calculations (Fe_1-Fe_2 was fixed at 1.43 Å). The last row lists the calculated energy with Fe_1-Fe_2 fixed at 1.40 Å.

P-Fe_1 interlayer spacing (Å)	Total energy (eV)	ΔE (eV)
1.06	−318411.46	1.89
1.04	−318412.48	0.87
1.01	−318413.35	0
0.99	−318410.35	3.00
1.01	−318411.97	1.38

These calculation results confirm the ARPEFS determination that the Fe_1-Fe_2 interlayer spacing is contracted from the bulk value for S/Fe but not for P/Fe. If the Fe_1-Fe_2 interlayer spacing is contracted to 1.40 Å for the P/Fe system, the total energy is raised by 1.39 eV. Similarly, if the Fe_1-Fe_2 interlayer spacing is fixed at the 1.43-Å bulk value for the S/Fe system, the total energy is raised by 3.82 eV.

V. CONCLUSION

Angle-resolved photoemission extended fine structure was used to determine the structure of $c(2\times2)$P/Fe(100). Photoemission data were collected normal to the (100) surface and 45° off-normal along the [011] direction at room temperature. A close analysis of the ARLP-based FT indicates that the P atoms adsorb in the high-coordination fourfold hollow sites. The FT analysis also allowed the bond distances to be estimated with surprisingly high accuracy. The curved-wave multiple scattering calculations that simulate the photoelectron diffraction confirmed the fourfold hollow adsorption site. By simultaneously fitting both ARPEFS data sets, the P atoms were determined to bond 1.02(2) Å above the first layer of Fe atoms. The Fe-P-Fe bond angle is thus 140.6°. Assuming the radius of the Fe atoms is 1.24 Å, the effective P radius is 1.03 Å. The inner potential was 15.0 eV. It was also determined that there was no relaxation of the first or second Fe layers from the bulk 1.43-Å interlayer spacing. To test this fitting method, each data set was fit

TABLE III. Variations of the total energy and the relative energy of SFe_9 with the S-Fe_1 interlayer distance from $X\alpha$ SW calculations (Fe_1-Fe_2 was fixed at 1.40 Å). The last row lists the calculated energy with Fe_1-Fe_2 fixed at 1.43 Å.

S-Fe_1 interlayer spacing (Å)	Total energy (eV)	ΔE (ev)
1.14	−319983.03	2.39
1.12	−319984.57	0.85
1.09	−319985.42	0
1.07	−319984.40	1.02
1.04	−319982.77	2.65
1.09	−319981.60	3.82

individually and these results were in good structural agreement.

Additionally, self-consistent-field $X\alpha$ scattered wave calculations were performed for the $c(2\times2)$P/Fe(100) and the $c(2\times2)$S/Fe(100) (Ref. 17) systems. These independent results are in excellent agreement with this P/Fe structure and the S/Fe structure previously published, confirming the ARPEFS determination that the Fe_1-Fe_2 interlayer spacing is contracted from the bulk value for S/Fe but not for P/Fe.

ACKNOWLEDGMENTS

This work was supported by the Director, Office of Energy Research, Office of Basic Energy Sciences, Chemical Sciences Division of the U.S. Department of Energy under Contract No. DE-AC03-76SF00098. It was performed at the Stanford Synchrotron Radiation Laboratory, which is supported by the Department of Energy's Office of Basic Energy Sciences.

[1] G. L. Krasko and G. B. Olson, Solid State Commun. **76**, 247 (1990).
[2] R. Wu, A. J. Freeman, and G. B. Olson, J. Mater. Res. **7**, 2403 (1992).
[3] S. Tang, A. J. Freeman, and G. B. Olson, Phys. Rev. B **47**, 2441 (1993).
[4] R. Wu, A. J. Freeman, and G. B. Olson, Phys. Rev. B **47**, 6855 (1993).
[5] R. Wu, A. J. Freeman, and G. B. Olson, Phys. Rev. B **50**, 75 (1994).
[6] B. Egert and G. Panzner, Surf. Sci. **118**, 345 (1982).
[7] S. Ohnishi, A. J. Freeman, and M. Weinert, Phys. Rev. B **28**, 6741 (1983).
[8] Y. Sakisaka, Y. N. Rhodin, B. Egert, and H. Grabke, Solid State Commun. **49**, 579 (1984).
[9] C. L. Fu and A. J. Freeman, Phys. Rev. B **35**, 925 (1987).
[10] S. R. Chubb and W. E. Pickett, Phys. Rev. B **38**, 10 227 (1988).
[11] R. Wu and A. J. Freeman, Phys. Rev. B **47**, 3904 (1993).
[12] R. Imbihl, R. J. Behm, G. Ertl, and W. Moritz, Surf. Sci. **123**, 129 (1982).
[13] K. O. Legg, F. Jona, D. W. Jepsen, and P. M. Marcus, Phys. Rev. B **16**, 5271 (1977).
[14] S. R. Chubb and W. E. Pickett, Solid State Commun. **62**, 19 (1987).
[15] K. O. Legg, F. Jona, D. W. Jepsen, and P. M. Marcus, Surf. Sci. **66**, 25 (1977).
[16] R. A. DiDio, E. W. Plummer, and W. R. Graham, J. Vac. Sci. Technol. A **2**, 983 (1984).
[17] X. S. Zhang, L. J. Terminello, S. Kim, Z. Q. Huang, A. E. Schach von Wittenau, and D. A. Shirley, J. Chem. Phys. **89**, 6538 (1988).
[18] D. P. Woodruff, D. Norman, B. W. Holland, N. V. Smith, H. H. Farrell, and M. M. Traum, Phys. Rev. Lett. **41**, 1130 (1978).
[19] J. J. Barton, C. C. Bahr, S. W. Robey, Z. Hussain, E. Umbach, and D. A. Shirley, Phys. Rev. B **34**, 3807 (1986).
[20] S. W. Robey, J. J. Barton, C. C. Bahr, G. Liu, and D. A. Shirley, Phys. Rev. B **35**, 1108 (1987).
[21] L. J. Terminello, K. T. Leung, Z. Hussain, T. Hayashi, X. S. Zhang, and D. A. Shirley, Phys. Rev. B **41**, 12 787 (1990).
[22] L. Q. Wang, A. E. Schach von Wittenau, L. S. Wang, Z. G. Ji, Z. Q. Huang, and D. A. Shirley, Phys. Rev. B **44**, 1292 (1991).
[23] Z. Q. Huang, Z. Hussain, W. T. Huff, E. J. Moler, and D. A. Shirley, Phys. Rev. B **48**, 1696 (1993).
[24] Z. Q. Huang, L. Q. Wang, A. E. Schach von Wittenau, Z. Hussain, and D. A. Shirley, Phys. Rev. B **47**, 13 626 (1993).
[25] J. J. Barton, C. C. Bahr, Z. Hussain, S. W. Robey, J. G. Tobin, L. E. Klebanoff, and D. A. Shirley, Phys. Rev. Lett. **51**, 272 (1983).
[26] J. J. Barton, Z. Hussain, and D. A. Shirley, Phys. Rev. B **35**, 933 (1987).
[27] S. D. Kevan, Ph.D. thesis, The University of California, Berkeley, LBL-11017 (1980).
[28] Z. Hussain, E. Umbach, D. A. Shirley, J. Stohr, and J. Feldhaus, Nucl. Instrum. Methods **195**, 115 (1982).
[29] C. A. Shell and J. C. Rivière, Surf. Sci. **40**, 149 (1973).
[30] J. J. Barton, Ph.D. thesis, The University of California, Berkeley, LBL-19215 (1985).
[31] J. J. Barton, S. W. Robey, and D. A. Shirley, Phys. Rev. B **34**, 778 (1986).
[32] Y. Zheng and D. A. Shirley, Chem. Phys. Lett. **203**, 114 (1993).
[33] Y. Chen, H. Wu, and D. A. Shirley (unpublished).
[34] J. J. Rehr and R. C. Albers, Phys. Rev. B **41**, 8139 (1990).
[35] A. Kaduwela, Ph.D. thesis, University of Hawaii at Manoa, Honolulu, 1991.
[36] M. Sagurton, E. L. Bullock, and C. S. Fadley, Surf. Sci. **182**, 287 (1987).
[37] R. E. Allen, G. P. Alldredge, and F. W. de Wette, J. Chem. Phys. **54**, 2605 (1971).
[38] V. L. Moruzzi, J. F. Janak, and A. R. Williams, *Calculated Electronic Properties of Metals* (Pergamon Press, New York, 1978).
[39] S. Tanuma, C. J. Powell, and D. R. Penn, Surf. Interface Anal. **20**, 77 (1993).
[40] K. A. R. Mitchell, Surf. Sci. **100**, 225 (1980).
[41] W. H. Press, S. A. Teukolsky, W. T. Vetterling, and B. P. Flannery, *Numerical Recipes in Fortran: The Art of Scientific Computing*, 2nd ed. (University Press, Cambridge, 1992).
[42] J. C. Slater, Phys. Rev. **81**, 385 (1951).
[43] K. H. Johnson, J. Chem. Phys. **45**, 3085 (1966).
[44] K. H. Johnson, Adv. Quantum Chem. **7**, 143 (1972).
[45] M. Cook and M. Karplus, J. Chem. Phys. **72**, 7 (1980).
[46] D. A. Case, M. Cook, and M. Karplus, J. Chem. Phys. **73**, 3294 (1980).
[47] M. E. Eberhart, K. H. Johnson, and D. Adler, Phys. Rev. B **26**, 3138 (1982).
[48] J. S.-Y. Chao and K. D. Jordan, J. Phys. Chem. **91**, 5578 (1987).
[49] M. Cook and C. T. White, Phys. Rev. B **38**, 9674 (1988).
[50] H. Adachi and M. Takano, J. Solid State Chem. **93**, 556 (1991).
[51] J. C. Slater, *Solid State and Molecular Theory: A Scientific Biography* (Wiley, New York, 1975).
[52] Jr. J. G. Norman, Mol. Phys. **31**, 1191 (1976).
[53] K. Schwarz, Phys. Rev. B **5**, 2466 (1972).